Ultrashort free-carrier lifetime in low-loss silicon nanowaveguides

Amy C. Turner-Foster,[1] Mark A. Foster,[2] Jacob S. Levy,[1] Carl B. Poitras,[1] Reza Salem,[2] Alexander L. Gaeta,[2] and Michal Lipson[1]*

[1]School of Electrical and Computer Engineering, Cornell University, Ithaca, NY 14853, USA
[2]School of Applied and Engineering Physics, Cornell University, Ithaca, NY 14853, USA
*lipson@ece.cornell.edu

Abstract: We demonstrate reduction of the free-carrier lifetime in a silicon nanowaveguide from 3 ns to 12.2 ps by applying a reverse bias across an integrated *p-i-n* diode. This observation represents the shortest free-carrier lifetime demonstrated to date in silicon waveguides. Importantly, the presence of the *p-i-n* structure does not measurably increase the propagation loss of the waveguide. We derive a figure of merit demonstrating equal dependency of the nonlinear phase shift on free-carrier lifetime and linear propagation loss.

© 2010 Optical Society of America

OCIS codes: (190.4390) Nonlinear optics, integrated optics; (130.7405) Wavelength conversion devices.

References and links

1. R. Claps, D. Dimitropoulos, Y. Han, and B. Jalali, "Observation of Raman emission in silicon waveguides at 1.54 micron," Opt. Express **10**(22), 1305–1313 (2002), http://www.opticsexpress.org/abstract.cfm?URI=OPEX-10-22-1305.
2. R. Claps, D. Dimitropoulos, and B. Jalali, "Stimulated Raman scattering in silicon waveguides," Electron. Lett. **38**(22), 1352–1354 (2002).
3. R. Claps, D. Dimitropoulos, V. Raghunathan, Y. Han, and B. Jalali, "Observation of stimulated Raman amplification in silicon waveguides," Opt. Express **11**(15), 1731–1739 (2003), http://www.opticsinfobase.org/abstract.cfm?URI=oe-11-15-1731.
4. T. K. Liang, and H. K. Tsang, "Role of free carriers from two-photon absorption in Raman amplification in silicon-on-insulator waveguides," Appl. Phys. Lett. **84**(15), 2745–2747 (2004).
5. R. Claps, V. Raghunathan, D. Dimitropoulos, and B. Jalali, "Influence of nonlinear absorption on Raman amplification in Silicon waveguides," Opt. Express **12**(12), 2774–2780 (2004), http://www.opticsexpress.org/abstract.cfm?URI=OPEX-12-12-2774.
6. Q. Xu, V. Almeida, and M. Lipson, "Time-resolved study of Raman gain in highly confined silicon-on-insulator waveguides," Opt. Express **12**(19), 4437–4442 (2004), http://www.opticsinfobase.org/abstract.cfm?URI=oe-12-19-4437.
7. J. I. Dadap, R. L. Espinola, R. M. Osgood, Jr., S. J. McNab, and Y. A. Vlasov, "Spontaneous Raman scattering in ultrasmall silicon waveguides," Opt. Lett. **29**(23), 2755–2757 (2004).
8. Q. Xu, V. R. Almeida, and M. Lipson, "Demonstration of high Raman gain in a submicrometer-size silicon-on-insulator waveguide," Opt. Lett. **30**(1), 35–37 (2005).
9. V. Raghunathan, R. Claps, D. Dimitropoulos, and B. Jalali, "Parametric Raman wavelength conversion in scaled Silicon waveguides," J. Lightwave Technol. **23**(6), 2094–2102 (2005).
10. R. Jones, H. Rong, A. Liu, A. Fang, M. Paniccia, D. Hak, and O. Cohen, "Net continuous wave optical gain in a low loss silicon-on-insulator waveguide by stimulated Raman scattering," Opt. Express **13**(2), 519–525 (2005), http://www.opticsinfobase.org/abstract.cfm?URI=oe-13-2-519.
11. R. Jones, A. Liu, H. Rong, M. Paniccia, O. Cohen, and D. Hak, "Lossless optical modulation in a silicon waveguide using stimulated Raman scattering," Opt. Express **13**(5), 1716–1723 (2005), http://www.opticsinfobase.org/oe/abstract.cfm?URI=oe-13-5-1716.
12. A. Liu, H. Rong, R. Jones, O. Cohen, D. Hak, and M. Paniccia, "Optical amplification and lasing by stimulated Raman scattering in Silicon waveguides," J. Lightwave Technol. **24**, 1440 (2006), http://www.opticsinfobase.org/JLT/abstract.cfm?URI=JLT-24-3-1440.
13. V. Sih, S. Xu, Y. H. Kuo, H. Rong, M. Paniccia, O. Cohen, and O. Raday, "Raman amplification of 40 Gb/s data in low-loss silicon waveguides," Opt. Express **15**(2), 357–362 (2007), http://www.opticsinfobase.org/oe/abstract.cfm?URI=oe-15-2-357.
14. A. Liu, H. Rong, M. Paniccia, O. Cohen, and D. Hak, "Net optical gain in a low loss silicon-on-insulator waveguide by stimulated Raman scattering," Opt. Express **12**(18), 4261–4268 (2004), http://www.opticsinfobase.org/oe/abstract.cfm?URI=oe-12-18-4261.

15. R. L. Espinola, J. I. Dadap, R. M. Osgood, Jr., S. J. McNab, and Y. A. Vlasov, "Raman amplification in ultrasmall silicon-on-insulator wire waveguides," Opt. Express **12**(16), 3713–3718 (2004), http://www.opticsinfobase.org/oe/abstract.cfm?URI=oe-12-16-3713.
16. Y. Liu, and H. K. Tsang, "Nonlinear absorption and Raman gain in helium-ion-implanted silicon waveguides," Opt. Lett. **31**(11), 1714–1716 (2006), http://www.opticsinfobase.org/ol/abstract.cfm?URI=ol-31-11-1714.
17. O. Boyraz, and B. Jalali, "Demonstration of a silicon Raman laser," Opt. Express **12**(21), 5269–5273 (2004), http://www.opticsinfobase.org/abstract.cfm?URI=oe-12-21-5269.
18. H. Rong, A. Liu, R. Nicolaescu, M. Paniccia, O. Cohen, and D. Hak, "Raman gain and nonlinear optical absorption measurements in a low-loss silicon waveguide," Appl. Phys. Lett. **85**(12), 2196–2198 (2004).
19. H. Rong, Y.-H. Kuo, S. Xu, A. Liu, R. Jones, M. Paniccia, O. Cohen, and O. Raday, "Monolithic integrated Raman silicon laser," Opt. Express **14**(15), 6705–6712 (2006), http://www.opticsinfobase.org/oe/abstract.cfm?URI=oe-14-15-6705.
20. H. Rong, A. Liu, R. Jones, O. Cohen, D. Hak, R. Nicolaescu, A. Fang, and M. Paniccia, "An all-silicon Raman laser," Nature **433**(7023), 292–294 (2005).
21. H. Rong, R. Jones, A. Liu, O. Cohen, D. Hak, A. Fang, and M. Paniccia, "A continuous-wave Raman silicon laser," Nature **433**(7027), 725–728 (2005).
22. H. K. Tsang, C. S. Wong, T. K. Liang, I. E. Day, S. W. Roberts, A. Harpin, J. Drake, and M. Asghari, "Optical dispersion, two-photon absorption and self-phase modulation in silicon waveguides at 1.5 µm wavelength," Appl. Phys. Lett. **80**(3), 416–418 (2002).
23. O. Boyraz, T. Indukuri, and B. Jalali, "Self-phase-modulation induced spectral broadening in silicon waveguides," Opt. Express **12**(5), 829–834 (2004), http://www.opticsinfobase.org/abstract.cfm?URI=oe-12-5-829.
24. E. Dulkeith, Y. A. Vlasov, X. Chen, N. C. Panoiu, and R. M. Osgood, Jr., "Self-phase-modulation in submicron silicon-on-insulator photonic wires," Opt. Express **14**(12), 5524–5534 (2006), http://www.opticsinfobase.org/abstract.cfm?URI=oe-14-12-5524.
25. I. W. Hsieh, X. Chen, J. I. Dadap, N. C. Panoiu, R. M. Osgood, S. J. McNab, and Y. A. Vlasov, "Ultrafast-pulse self-phase modulation and third-order dispersion in Si photonic wire-waveguides," Opt. Express **14**(25), 12380–12387 (2006), http://www.opticsinfobase.org/abstract.cfm?URI=oe-14-25-12380.
26. R. Salem, M. A. Foster, A. C. Turner, D. F. Geraghty, M. Lipson, and A. L. Gaeta, "All-optical regeneration on a silicon chip," Opt. Express **15**(12), 7802–7809 (2007), http://www.opticsinfobase.org/abstract.cfm?URI=oe-15-12-7802.
27. I. W. Hsieh, X. Chen, J. I. Dadap, N. C. Panoiu, R. M. Osgood, Jr., S. J. McNab, and Y. A. Vlasov, "Cross-phase modulation-induced spectral and temporal effects on co-propagating femtosecond pulses in silicon photonic wires," Opt. Express **15**(3), 1135–1146 (2007), http://www.opticsinfobase.org/abstract.cfm?URI=oe-15-3-1135.
28. R. L. Espinola, J. I. Dadap, R. M. Osgood, Jr., S. J. McNab, and Y. A. Vlasov, "C-band wavelength conversion in silicon photonic wire waveguides," Opt. Express **13**(11), 4341–4349 (2005), http://www.opticsinfobase.org/abstract.cfm?URI=oe-13-11-4341.
29. H. Fukuda, K. Yamada, T. Shoji, M. Takahashi, T. Tsuchizawa, T. Watanabe, J. Takahashi, and S. Itabashi, "Four-wave mixing in silicon wire waveguides," Opt. Express **13**(12), 4629–4637 (2005), http://www.opticsinfobase.org/abstract.cfm?URI=oe-13-12-4629.
30. H. Rong, Y.-H. Kuo, A. Liu, M. Paniccia, and O. Cohen, "High efficiency wavelength conversion of 10 Gb/s data in silicon waveguides," Opt. Express **14**(3), 1182–1188 (2006), http://www.opticsinfobase.org/abstract.cfm?URI=oe-14-3-1182.
31. M. A. Foster, A. C. Turner, J. E. Sharping, B. S. Schmidt, M. Lipson, and A. L. Gaeta, "Broad-band optical parametric gain on a silicon photonic chip," Nature **441**(7096), 960–963 (2006).
32. K. Yamada, H. Fukuda, T. Tsuchizawa, T. Watanabe, T. Shoji, and S. Itabashi, "All-optical efficient wavelength conversion using silicon photonic wire waveguide," IEEE Photon. Technol. Lett. **18**(9), 1046–1048 (2006).
33. Y.-H. Kuo, H. Rong, V. Sih, S. Xu, M. Paniccia, and O. Cohen, "Demonstration of wavelength conversion at 40 Gb/s data rate in silicon waveguides," Opt. Express **14**(24), 11721–11726 (2006), http://www.opticsinfobase.org/abstract.cfm?URI=oe-14-24-11721.
34. M. A. Foster, A. C. Turner, R. Salem, M. Lipson, and A. L. Gaeta, "Broad-band continuous-wave parametric wavelength conversion in silicon nanowaveguides," Opt. Express **15**(20), 12949–12958 (2007), http://www.opticsinfobase.org/abstract.cfm?URI=oe-15-20-12949.
35. R. Salem, M. A. Foster, A. C. Turner, D. F. Geraghty, M. Lipson, and A. L. Gaeta, "Signal regeneration using low power four-wave mixing on silicon chip," Nat. Photonics **2**(1), 35–38 (2008).
36. A. C. Turner, M. A. Foster, A. L. Gaeta, and M. Lipson, "Ultra-low power parametric frequency conversion in a silicon microring resonator," Opt. Express **16**(7), 4881–4887 (2008), http://www.opticsinfobase.org/oe/abstract.cfm?URI=oe-16-7-4881.
37. M. A. Foster, A. C. Turner, M. Lipson, and A. L. Gaeta, "Nonlinear optics in photonic nanowires," Opt. Express **16**(2), 1300–1320 (2008).
38. Q. Lin, J. Zhang, P. M. Fauchet, and G. P. Agrawal, "Ultrabroadband parametric generation and wavelength conversion in silicon waveguides," Opt. Express **14**(11), 4786–4799 (2006), http://www.opticsinfobase.org/abstract.cfm?URI=oe-14-11-4786.
39. D. Dimitropoulos, R. Jhaveri, R. Claps, J. C. S. Woo, and B. Jalali, "Lifetime of photogenerated carriers in silicon-on-insulator rib waveguides," Appl. Phys. Lett. **86**(7), 071115 (2005).
40. M. Waldow, T. Plötzing, M. Gottheil, M. Först, J. Bolten, T. Wahlbrink, and H. Kurz, "25ps all-optical switching in oxygen implanted silicon-on-insulator microring resonator," Opt. Express **16**(11), 7693–7702 (2008), http://www.opticsinfobase.org/oe/abstract.cfm?URI=oe-16-11-7693.

41. N. M. Wright, D. J. Thomson, K. L. Litvinenko, W. R. Headley, A. J. Smith, A. P. Knights, J. H. B. Deane, F. Y. Gardes, G. Z. Mashanovich, R. Gwilliam, and G. T. Reed, "Free carrier lifetime modification for silicon waveguide based devices," Opt. Express **16**(24), 19779–19784 (2008), http://www.opticsinfobase.org/oe/abstract.cfm?URI=oe-16-24-19779.
42. P. Apiratikul, A. M. Rossi, and T. E. Murphy, "Nonlinearities in porous silicon optical waveguides at 1550 nm," Opt. Express **17**(5), 3396–3406 (2009), http://www.opticsinfobase.org/oe/abstract.cfm?URI=oe-17-5-3396.
43. K. Preston, P. Dong, B. Schmidt, and M. Lipson, "High-speed all-optical modulation using polycrystalline silicon microring resonators," Appl. Phys. Lett. **92**(15), 151104 (2008).
44. T. J. Johnson, and O. J. Painter, "Passive Modification of Free Carrier Lifetime in High-Q Silicon-on-Insulator Optics," in *Conference on Lasers and Electro-Optics/International Quantum Electronics Conference*, OSA Technical Digest (CD) (Optical Society of America, 2009), paper CFF4. http://www.opticsinfobase.org/abstract.cfm?URI=CLEO-2009-CFF4
45. V. R. Almeida, C. A. Barrios, R. R. Panepucci, and M. Lipson, "All-optical control of light on a silicon chip," Nature **431**(7012), 1081–1084 (2004).
46. S. F. Preble, Q. Xu, B. S. Schmidt, and M. Lipson, "Ultrafast all-optical modulation on a silicon chip," Opt. Lett. **30**(21), 2891–2893 (2005), http://www.opticsinfobase.org/abstract.cfm?URI=ol-30-21-2891.
47. Q. Xu, B. Schmidt, S. Pradhan, and M. Lipson, "Micrometre-scale silicon electro-optic modulator," Nature **435**(7040), 325–327 (2005).
48. V. R. Almeida, R. R. Panepucci, and M. Lipson, "Nanotaper for compact mode conversion," Opt. Lett. **28**(15), 1302–1304 (2003).
49. Z. Vardeny, and J. Tauc, "Hot-carrier thermalization in amorphous silicon," Phys. Rev. Lett. **46**(18), 1223–1226 (1981).
50. D. Dimitropoulos, S. Fathpour, and B. Jalali, "Limitations of active carrier removal in silicon Raman amplifiers and lasers," Appl. Phys. Lett. **87**(26), 261108 (2005).

1. Introduction

Nonlinear optical processes in silicon such as Raman scattering [1–16] and oscillation [17–21], self- [22–26] and cross-phase modulation [27], and four-wave mixing [28–37] have enabled a number of demonstrations of devices that can operate at low powers, have small, micron-scale footprints, and can be fully integrated along with electronics in a CMOS-platform. All of these experiments are enabled by the beneficial material properties of silicon in the telecommunications bands including low linear material losses, high linear refractive index, and large nonlinear refractive index. However, the efficacy of these processes is limited by nonlinear loss mechanisms.

The two major nonlinear optical loss mechanisms in silicon waveguides at communications wavelengths are two-photon absorption (TPA) and free-carrier absorption (FCA) [10,38]. Two-photon absorption is a result of the proximity of the band edge to communication wavelengths and is unavoidable when operating in this wavelength range. Free-carriers are generated via TPA, and these carriers can efficiently absorb subsequent photons through linear absorption. For most demonstrations, the severity of the FCA mechanism is determined by the lifetime of the photo-excited free-carriers present in the silicon. The free-carrier lifetime is on the order of microseconds in lightly doped bulk silicon [39]. A number of techniques have been applied to reduce the free-carrier lifetime in silicon waveguides. These techniques fall into three main categories: material modification including ion implantation [16,40,41], porous silicon [42] and polysilicon [43]; increasing surface recombination through a reduction in waveguide dimensions [15,39,44–46] or surface chemistry modification [44]; and most prominently carrier removal through integration of a *p-i-n* diode across the waveguide [20,21,30,33,46]. The shortest previously demonstrated free-carrier lifetime is 15 ps through ion implantation [40]; however these waveguides suffer from an additional 68 dB/cm propagation loss due to the implantation. This additional propagation loss offsets any benefit of reduced FCA for nonlinear optical interactions.

Here, by integrating a *p-i-n* diode across a silicon nanowaveguide, we demonstrate a free-carrier lifetime of 12.2 ps, which is the shortest lifetime observed to date in silicon waveguides or resonators and is 100 times shorter than any other demonstrations in silicon waveguides with an integrated *p-i-n* for carrier removal [20]. As previously predicted [39], this large reduction in lifetime is enabled by the submicron cross-sectional dimensions of the device. The implementation of this device is accompanied by a negligible increase in propagation loss, in agreement with other works [20,39], and we measure an overall propagation loss of ~2 dB/cm in our waveguides with integrated *p-i-n* diodes. Furthermore,

we derive a figure of merit for nonlinear optical processes in silicon waveguides, which shows the equal dependence of the maximum nonlinear performance on the free-carrier lifetime and propagation loss.

2. Device design and fabrication

The cross-section of the rib waveguide consists of a silicon channel waveguide on top of a 40-nm silicon slab (Fig. 1). The waveguide width is 660 nm, and the height of the silicon layer at the thickest part of the waveguide is 295 nm. In order to design the *p-i-n* geometry of the device, we follow the general design of [46,47] with a highly doped *p*-type region on one side of the waveguide and a highly doped *n*-type region on the opposite side (Fig. 1). The light propagates in the TE-like mode that is concentrated in the intrinsic central region of the waveguide. These doped regions are located 300 nm away from the edges of the waveguide and run the entire 1.2-cm length of the waveguide (Fig. 2). The *p-i-n* diode is not present near the nanotapers [48] which are used to couple light into and out of the waveguide.
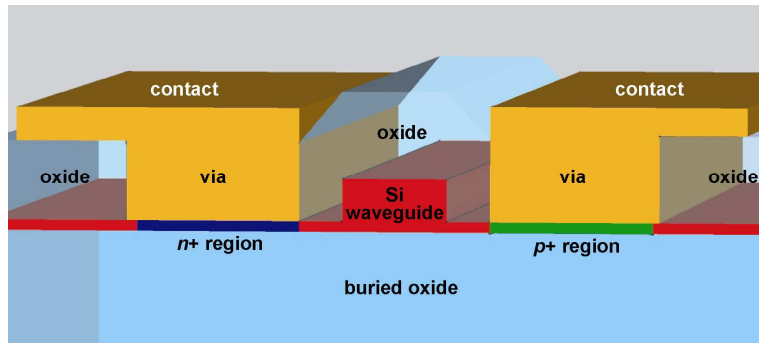

Fig. 1. Cross-sectional schematic of *p-i-n* waveguide device. The device consists of a silicon rib waveguide on the SOI platform. The waveguide has silicon dioxide cladding, *p* + and *n* + doping in the slab region on either side, and vias and contacts to the doped regions.

The device is fabricated on a silicon-on-insulator (SOI) wafer with a buried oxide of 3 µm and a silicon thickness of 295 nm. The waveguide is patterned using hydrogen silsesquioxane (HSQ) with an electron-beam lithography tool. The waveguides are etched to a depth of 255 nm in a Cl/BCl$_3$ environment using an inductively-coupled plasma reactive-ion-etching (ICP-RIE) tool. The *p* + and *n* + doping regions are defined and implanted with boron and arsenic, respectively, to create concentrations of 10^{19} cm^{-3}. A 1-µm layer of silicon dioxide is deposited on the sample using plasma-enhanced chemical vapor deposition (PECVD), and the devices are then annealed for dopant activation. Using Poly (methyl methacrylate) (PMMA), via regions are defined, etched, and 40 nm of nickel is deposited using electron-beam evaporation. The sample is annealed using a rapid-thermal annealing tool at 500°C for 30 seconds to form nickel silicide (NiSi). The contacts are then patterned, and 1 µm of aluminum is evaporated using electron-beam evaporation.

An optical microscope image and a schematic of the final devices are shown in Fig. 2. The *p* + and *n* + regions, the vias, and the contacts extend the entire length of the waveguide except for in the proximity of the nanotaper, and where the *p* + contact crosses the waveguide. Here the contact and via for the *n* + region are not extended in order to avoid shorting the device, but the *n* + doping region is extended as depicted in the schematic.
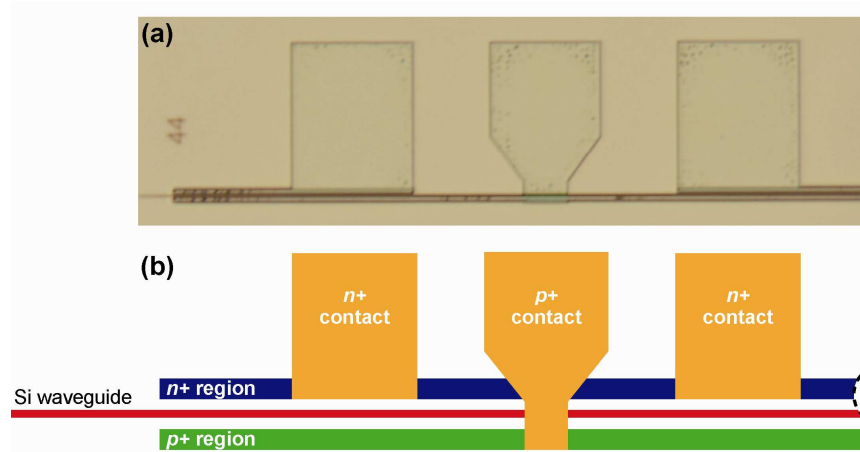
Fig. 2. Top view (a) optical microscope image and (b) schematic of *p-i-n* waveguide. The two outer contacts are connected to the *n* + region with etched vias, whereas the center contact is only connected to the *p* + region. The *n* + region underneath the *p* + contact is electrically isolated by a 1-µm layer of silicon dioxide.

3. Measurement of the free-carrier lifetime

To determine the free-carrier lifetime of the rib waveguide, we perform a pump-probe measurement as depicted in Fig. 3. A 9.1-ps-long pump pulse with 38-MHz repetition rate and a center wavelength of 1554 nm is amplified in a low-noise erbium-doped fiber amplifier (EDFA) to a sufficiently high peak power to generate free-carriers through TPA. This pump pulse is modulated at 20 kHz with an electro-optic modulator and coupled into the TE-like mode of our waveguide. The probe pulse at a center wavelength of 1537 nm is 4.7-ps-long and also has a 38 MHz repetition rate. This probe is sent through a free-space variable-delay stage and combined with the pump pulse to be coupled into the TE-like mode of the silicon waveguide. The average (peak) powers of the pump and probe inside the waveguide are 0.5 mW (2.9 W) and 24 µW (0.13 W), respectively. The output of the waveguide is coupled into a single-mode fiber, the light centered at the probe wavelength is filtered and sent to a detector and a lock-in amplifier to monitor the nonlinear effects of the pump on the probe. Additionally, the power in the FWM-generated wave at 1561 nm is measured to determine the cross-correlation of the pump and probe. Monitoring the 20-kHz modulation transferred to the probe as a function of delay yields a curve that is shaped by the combined effects of TPA, parametric amplification and FCA. To determine solely the contribution from FCA, we remove the effects due to TPA and parametric amplification by using the cross-correlation to resolve the shape of these instantaneous contributions. Since the free-carriers accumulate over the duration of the pump pulse, the magnitude of the instantaneous contributions is determined by the lock-in signal from when the probe is in front of the pump where the effects of TPA and parametric amplification dominate over free-carrier effects. For the 0V biased measurement, the maximum TPA was 2.2 times larger than the maximum FCA and the magnitude of the maximum parametric amplification was 1.8 times larger than the magnitude of the maximum FCA.
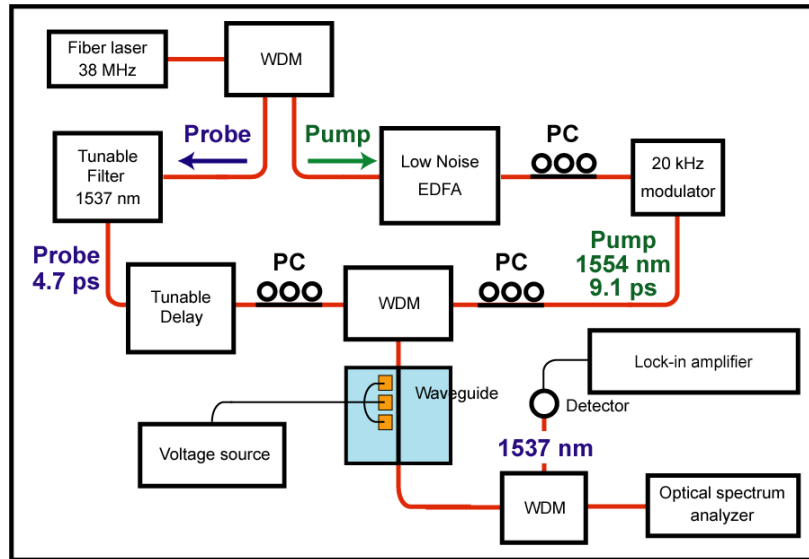
Fiber laser 38 MHz — WDM

Probe ← **Pump** → Low Noise EDFA — **PC** ooo — 20 kHz modulator

Tunable Filter 1537 nm

Probe 4.7 ps — Tunable Delay — **PC** ooo — WDM — **PC** ooo — **Pump 1554 nm 9.1 ps**

Voltage source — Waveguide

Lock-in amplifier — Detector

1537 nm

WDM — Optical spectrum analyzer

Fig. 3. A pump-probe experiment is performed to determine the free-carrier lifetime of a silicon waveguide as a function of applied reverse-bias.

We measure the lifetime of free-carriers for a range of reverse-bias values from 0 to 15 V and obtain a reduction in the lifetime from 3 ns to 12.2 ps. Figure 4(a) shows the free-carrier concentration as a function of time relative to the end of the pump pulse for various applied voltages. We determine the end of the pump pulse by the delay at which the FWM cross-correlation signal becomes negligible which also corresponds to the point of maximum free-carrier concentration. For these measurements, this was 10 ps from the delay at which the two pulses are perfectly overlapped. We observe a rapid initial reduction in the free-carrier density due to the high-temperature of the photo-generated carriers [49] followed by a slow decline in free-carrier density once the carriers reach a thermal equilibrium. As shown, the application of a reverse-bias voltage greatly increases this secondary rate of decay. Each of these curves is fit to a double exponential, and the effective free-carrier lifetime is extracted. The lifetime is defined here as when the absorption on the probe due to free carriers has reduced to the $1/e$ value of the overall decay.

Figure 4(b) shows the experimental free-carrier lifetime as a function of reverse bias obtained from Fig. 4(a). As is shown, significant reductions in the free-carrier lifetime are observed even for relatively small applied voltages. The shortest lifetime of 12.2 ps is observed at the largest applied voltage of 15 V. The red line is an exponential fit to serve as a visual guide. To verify the absence of carrier screening effects, the free-carrier lifetime was measured for various peak pump powers inside the waveguide at a 9-V bias showing no observable dependence on power [50]. This measurement is shown in the inset of Fig. 4(b). The peak power range corresponds to an estimated peak carrier density ranging from 2×10^{16} to 9×10^{16} cm^{-3}. We estimate carrier screening to play a role in our device at carrier densities of 10^{17} cm^{-3}.
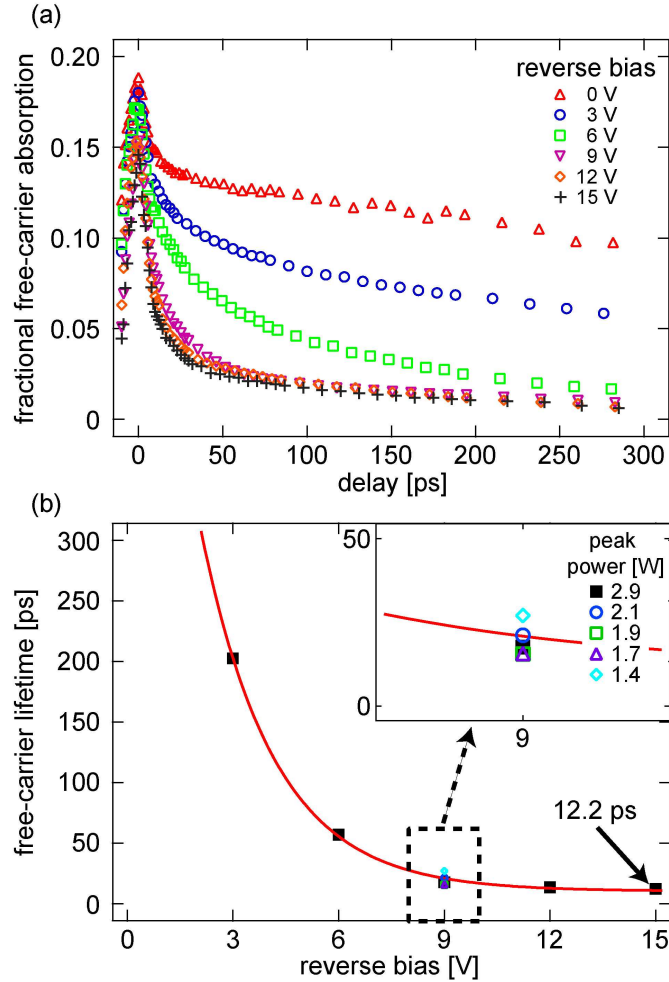
Fig. 4. Experimentally measured free-carrier lifetime as a function of reverse bias in silicon photonic waveguides optimized for phase matching with an integrated *p-i-n* diode for reduction of nonlinear loss. (a) The free-carrier concentration as a function of time for different reverse biases. (b) The measured free-carrier lifetime as a function of reverse bias, illustrating the ability to reduce the free-carrier lifetime to 12.2 ps. The lifetime for 9-V bias was measured as a function of pump power as shown in the inset.

4. Figure of merit for nonlinear optical processes in silicon waveguides

To improve the efficiency of parametric processes in silicon, the reduction of both the free-carrier lifetime and the linear propagation loss are equally important. Previously, there have been a number of demonstrations that have focused on reducing either one of these loss mechanisms at the expense of increasing the other. The efficiency of $\chi^{(3)}$ nonlinear optical processes can be defined using the nonlinear phase shift, and here we derive a figure of merit for our system based on maximizing this parameter. This figure of merit demonstrates the equal dependence of the nonlinear phase shift on both linear propagation loss and free-carrier lifetime. We also show that our derived figure of merit matches very well to direct numerical simulations of the nonlinear phase shift in our system.

The nonlinear phase shift (φ_{NL}) for a waveguide can be expressed as:

$$\varphi_{NL} = \frac{2\pi n_2}{\lambda} \int_0^L I(z)dz, \tag{1}$$

where L is the effective interaction length, λ is the free-space wavelength of the light, and n_2 is the nonlinear refractive index coefficient. $I(z)$ is the intensity of the light wave in the material and is a function of propagation length z due to the presence of multiple loss mechanisms. We model this dependence using the following differential equation:

$$\frac{dI(z)}{dz} = -\left[\alpha_{lin} + \beta_{TPA} I(z) + \alpha_{FCA} I^2(z) \right] I(z), \tag{2}$$

where α_{lin} is the linear propagation loss, β_{TPA} is the two-photon absorption coefficient, and

$$\alpha_{FCA} = 1.45 \cdot 10^{-21} [\mathrm{m}^2] \left(\frac{\lambda}{1.55 \cdot 10^{-6}[\mathrm{m}]} \right)^2 \frac{\beta_{TPA} \tau_{eff} \lambda}{2hc}, \tag{3}$$

is the free-carrier absorption coefficient [5], where τ_{eff} is the effective free-carrier lifetime, h is Planck's constant, c is the speed of light in vacuum, and m denotes that the units of the numeric quantities are in meters. To isolate the impact of free-carrier absorption on achievable nonlinear phase shift, we solve Eq. (2) neglecting the terms from linear propagation loss and two-photon absorption, which yields,

$$I(z) = \frac{I_0}{\sqrt{1 + 2I_0^2 \alpha_{FCA} z}}, \tag{4}$$

where I_0 is the intensity of the light wave at $z = 0$. Substituting Eq. (4) into Eq. (1) yields,

$$\varphi_{NL} = \frac{2\pi n_2}{\lambda I_0 \alpha_{FCA}} \left[\sqrt{1 + 2I_0^2 \alpha_{FCA} L} - 1 \right]. \tag{5}$$

In an ideal nonlinear device, increasing the intensity would always increase the nonlinear phase shift. However in our device, we see that in the limit where the intensity approaches infinity the phase shift saturates due to free-carrier absorption,

$$\varphi_{\max} \equiv \lim_{I_0 \to \infty} \varphi_{NL} = \frac{2\pi n_2 \sqrt{2L}}{\lambda \sqrt{\alpha_{FCA}}}. \tag{6}$$

We can see from Eq. (6) that there is a maximum achievable nonlinear phase shift $\varphi_{\max}$, which is determined primarily by the interaction length. The maximum interaction length is limited by linear propagation loss ($L \propto 1/\alpha_{lin}$) so that by reducing this loss we can improve the nonlinear performance of our waveguide. The free-carrier absorption is the other parameter of interest, and from Eq. (3) we see that $\alpha_{FCA} \propto \tau_{eff}$. Combining these two dependencies yields,

$$\varphi_{\max} \propto \frac{1}{\sqrt{\tau_{eff} \alpha_{lin}}}. \tag{7}$$

Since linear propagation loss is typically quoted in units of dB/cm, we instead use α_{dB} and define our figure of merit (FOM) as,

$$FOM \equiv \frac{1}{\sqrt{\tau_{eff} \alpha_{dB}}}. \tag{8}$$

This FOM shows that the linear propagation loss and effective free-carrier lifetime play equal roles in their effect on the maximum nonlinear phase shift. Note that since this

derivation does not include two-photon absorption and linear propagation loss, it subsequently neglects the interplay between the three loss mechanisms. To determine the validity of this FOM, we perform full numerical modeling including the combined effects of linear propagation loss, two-photon absorption and free-carrier absorption and solve for the maximum nonlinear phase shift as a function of linear propagation loss and free-carrier lifetime.
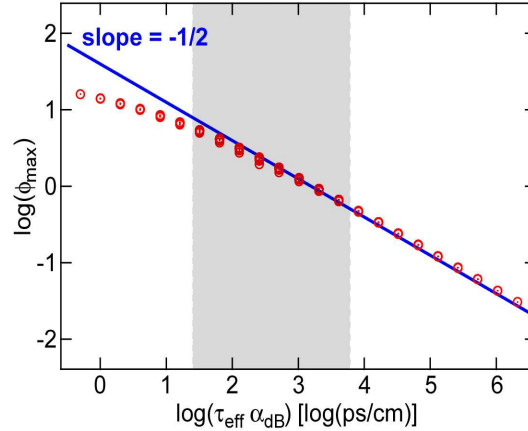

Fig. 5. Numerical solution of the maximum nonlinear phase shift for different values of linear propagation loss and free-carrier lifetime (circles). The blue line is plotted with a slope of –1/2 showing the consistency of the numerical solutions with the derived figure of merit [Eq. (8)]. The gray region depicts the range of linear propagation loss and free-carrier lifetime values where most silicon nanowaveguide nonlinear optical processes are performed. Note that the individual values of the free-carrier lifetime and linear propagation loss are varied by orders of magnitude, but provided that the product is constant, the maximum nonlinear phase shift is nearly identical as depicted by the multiple overlapping data points (circles) at each x value.

We analyze the validity of the proposed FOM for the dependence of the phase shift with linear loss and free-carrier lifetime by comparing the FOM with numerical solutions (Fig. 5) and show very small deviations. In Fig. 5 the linear propagation loss and the free-carrier lifetime are varied from 0.1 dB/cm to 51 dB/cm and from 5 ps to 41 ns, respectively, both in powers of 2, and the maximum nonlinear phase shift is numerically determined at every combination of these two variables. We assume the nonlinearity of silicon to be $n_2 = 6.5 \times 10^{-14}$ cm^2/W and the two-photon absorption coefficient to be $\beta_{TPA} = 0.7$ cm/GW [31–33] at the wavelength $\lambda = 1550$ nm. It is important to note that when the individual values of the free-carrier lifetime and linear propagation loss are varied by orders of magnitude, provided that the product is constant, the maximum nonlinear phase shift remains constant as is depicted by the multiple data points at each x value in Fig. 5. The line plotted in Fig. 5 represents a function with a slope of –1/2 on a log-log plot. This corresponds to a $y = 1/\sqrt{x}$ dependency, consistent with our FOM as defined in Eq. (8). We see that for very small values of free-carrier absorption and linear propagation loss, the numerical model deviates from the FOM, however the trend of improved nonlinear phase shift with decreased linear propagation loss and decreased free-carrier lifetime is preserved. In addition, most nonlinear optical demonstrations in silicon fall within the gray range depicted in Fig. 5, where deviation from the FOM is negligible.

While other research has focused on reducing either one of these loss mechanisms for nonlinear optical processes in silicon waveguides, here in our demonstration we are able to reduce the free-carrier lifetime to the shortest value demonstrated to date while simultaneously maintaining a very low linear propagation loss of ~2 dB/cm. We compare the performance of our device to those previously demonstrated in Table 1. Our waveguides exhibit the best demonstrated FOM to date of 0.202 cm$^{1/2}$·ps$^{-1/2}$, which reflects the greatest

reduction of the free-carrier lifetime (12.2 ps). This corresponds to the left edge of the gray region in Fig. 5 (1.38 [log(ps/cm)]).

Table 1. Performance comparison of silicon waveguides and resonators for nonlinear interactions

Reference	Reduction Technique	Geometry	α_{dB} [dB/cm]	τ_{eff} [ps]	FOM [cm$^{1/2}$·ps$^{-1/2}$]
this work	*p-i-n* and submicron dimensions	waveguide	2	12.2	**0.202**
[20,21,30,33]	*p-i-n*	waveguide	0.35	1200	0.049
[46]	*p-i-n*	ring	6.8 *	50	0.054
[16]	ion implantation	waveguide	2.3	1900	0.015
[40]	ion implantation	ring	100	15	0.026
[41]	ion implantation	waveguide	1.2	780	0.033
[42]	porous Si	waveguide	9	200	0.024
[43]	polysilicon	ring	10	135	0.027
[15]	submicron dimensions	waveguide	3.6	770	0.019
[45]	submicron dimensions	ring	77 *	450	0.005
[44]	surface passivation	disk	1.7	300	0.044

* calculated from cavity quality factor assuming critical coupling

5. Conclusion

We demonstrate significant reduction of free-carrier lifetimes in silicon waveguides to 12.2 ps with a negligible increase in propagation loss. This observation currently represents the shortest free-carrier lifetime demonstrated in silicon waveguides. In addition, we derive a figure of merit demonstrating the equal role between linear propagation loss and free-carrier absorption on the efficiency of nonlinear optical processes in silicon. This figure of merit reveals the importance of designing silicon waveguides with both short free-carrier lifetimes and low linear propagation losses. The device demonstrated here has the best measured figure-of-merit to date of 0.202 cm$^{1/2}$·ps$^{-1/2}$.

Acknowledgements